Dynamic Analysis of a Rotating Composite Shaft

R. Sino, Thouraya Baranger, E. Chatelet, G. Jacquet

Dynamic Analysis of a Rotating Composite Shaft

R. Sino, T.N. Baranger, E. Chatelet, G. Jacquet

PII: S0266-3538(07)00268-0
DOI: 10.1016/j.compscitech.2007.06.019
Reference: CSTE 3759

To appear in: *Composites Science and Technology*

Received Date: 6 December 2006
Revised Date: 18 June 2007
Accepted Date: 21 June 2007

Please cite this article as: Sino, R., Baranger, T.N., Chatelet, E., Jacquet, G., Dynamic Analysis of a Rotating Composite Shaft, *Composites Science and Technology* (2007), doi: 10.1016/j.compscitech.2007.06.019

Dynamic Analysis of a Rotating Composite Shaft

R. Sino [a], T. N. Baranger [a,b,*], E. Chatelet [a], G. Jacquet [a]

[a] *Laboratoire de Mécanique des Contacts et des Structures. LaMCoS, INSA-Lyon, CNRS UMR5259, F69621, France*

[b] *Université de Lyon, Lyon, F69003, France; Université Lyon1, Villeurbanne, F69622, France.*

Abstract

This paper is concerned with the dynamic instability of an internally damped rotating composite shaft. A homogenized finite element beam model, which takes into account internal damping, is introduced and then used to evaluate natural frequencies and instability thresholds. The influence of laminate parameters: stacking sequences, fiber orientation, transversal shear effect on natural frequencies and instability thresholds of the shaft are studied. The results are compared to those obtained by using equivalent modulus beam theory (EMBT), modified EMBT and Layerwise beam theory (LBT), which are used in the literature. This parametric study shows that shaft instability thresholds can be very sensitive to laminate parameters.

Key words: Rotordynamics, Composite Shaft, Damping, Stability, Threshold speed, Transversal shear, Finite element, Beam theory.

1 INTRODUCTION

Composite materials have interesting properties such as high strength to weight ratio, compared to metals, which make them very attractive for rotating systems. Attempts are being made to replace metal shafts by composite ones in many applications: drive shafts for helicopters, centrifugal separators, and

* Corresponding author. Tel.: 33 4 72 43 85 65; fax: 33 4 72 43 89 30
Email address: thouraya.baranger@insa-lyon.fr (T. N. Baranger).
URL: http://lamcos.insa-lyon.fr (G. Jacquet).

cylindrical tubes for the automotive and marine industries (Zorzi and Giordano [27], Darlow [4], Gupta and Singh [12,14,15], Chatelet [2]). They also provide designers with the possibility of obtaining predetermined behaviors, in terms of position of critical speeds, by changing the arrangement of the different composite layers: orientation and number of plies (Bauchau [1], Gubran and Gupta [19], Chatelet [2] and Pereira [6]). On the other hand, these materials have relatively high-damping characteristics. For a rotor made with composite materials, internal damping is much more significant than when associated with a metal rotor. Unfortunately, such damping may cause instability as shown by Wettergren [24].

Accurate prediction of damping characteristics of rotor systems is therefore fundamental in the design of rotating machines as it provides estimations on safe-ranges of speeds of rotation. Over the last few years, many studies have focused on predicting critical speeds, natural frequencies, unbalance responses and, in particular, instability thresholds. Newkirk [10] observed that rotor-disk systems would undergo violent whirling at the first natural frequency at speeds above the first critical speed. Kimball [7] showed that internal damping destabilizes the whirling motion if the rotation speed of the rotor exceeds the first critical speed. In addition, Bucciarelli [9] showed that the instability criterion based on the ratio of energy dissipated between internal and external damping is inaccurate and that internal forces can produce instability by coupling spin and whirl motions. Classical results have been obtained and showed that rotor stability is improved by increasing external damping, whereas increasing internal damping may reduce the instability threshold. However, most of the published studies deal with metal rotating structures and remain exclusively numerical without precise estimations of internal damping.

Several finite element formulations have been performed for the analysis of composite shafts. These formulations are based on homogenized beam and shell theories. The equivalent modulus beam theory (EMBT), which is widely used for the dynamic analysis of composite shafts, was firstly introduced by Tsai [23]. With this approach, equivalent longitudinal Young and in-plane shear moduli are identified by using laminate theory for symmetrical stacking. Then, classical beam theory can be used to model the shaft, see Pereira [6] and Singh and Gupta [14]. This approach has many limitations which are summarized by Singh and Gupta in [12]. They studied the natural frequencies and damping ratios in flexural modes of cylindrical laminate tubes and compared shell and EMBT models for symmetric laminate stacking, concluding that in the case of the tube configurations usually used in composite shaft applications, the differences in flexural frequencies between the two models are negligibly small. Using shell theory in [13], the same authors, showed that the modal loss factors are more sensitive to parametric (laminate stacking, angle orientations, etc.) changes than frequency values. They also presented in [15] a comparison between EMBT theory and Layerwise Beam Theory (LBT)

for symmetric and asymmetric stacking. They showed that LBT is more efficient that EMBT because it takes into account the effect of changed stacking, thickness shear deformation and bending-stretching coupling. However, LBT requires the development of a complex beam element with a high number of degrees of freedom dependent on the number of layers, making the method too expensive. Recently, Gubran and Gupta presented in [19] a modified EMBT method which takes into account the effects of a stacking sequence and different coupling mechanisms. They considered a Graphite/Epoxy shaft simply supported on rigid bearings and compared the first three frequencies with those obtained by using the LBT method. In spite of its simplicity, the natural frequencies obtained using modified EMBT excluding different coupling effects agree well with those obtained using LBT and those reported in the literature. In these cited works, the internal damping, is not often taken into account, except in [12] where viscoelastic material damping is assumed.

In this paper, a Simplified Homogenized Beam Theory (SHBT) is used to analysis the sensitivity of the frequencies and instability thresholds regarding shear effect, stacking order and fiber orientation. In this approach, the homogenized beam parameters such as flexural and shear stiffness are evaluated using an energy formulation that simultaneously considers Young's modulus, shear modulus, specific damping capacity, the distance to the shaft axis orientation and the thickness of each layer of the rotor. Flexural warping is determined by solving a boundary value problem defined on the cross-section, as mentioned in Nouri and Gay [11], then the shear corrector factor is evaluated. However, the formulation is simplified by assuming that the mechanical coupling effects, induced by the nonsymmetrical stacking of layers, are negligible. This approach is connected to that developed by Gubran and Gupta in [19] under the same assumption.

In the following, an outline of the formulation is presented. In section 2, equations of motion of rotordynamics with and without internal damping are presented and compared. In section 3, the orthotropic properties of a layer component of a composite shaft are presented. In section 4, a homogenized beam theory is developed and elastic energy and dissipative virtual work are given. Then, in section 5, the homogenized beam parameters are expressed as a function of the layer parameters. Numerical applications are presented in section 6. In the first one, frequencies are compared with those obtained by Gubran and Gupta in [19] using the modified EMBT and LBT methods. The second application is that presented in the work of Pereira [6]. The sensitivity of the shaft frequencies and instability thresholds regarding stacking order and fiber orientations are outlined. These results are also compared to those obtained from a classical equivalent modulus beam theory.

2 Rotordynamics

In the fixed frame, the following equations of motion are associated with a rotor made of an isotropic material (Lalanne [8]):

$$[M]\left\{\ddot{d}\right\} + [C(\Omega)]\left\{\dot{d}\right\} + [K]\{d\} = \{F(t)\} \tag{1}$$

where $[M]$ is the symmetric mass matrix, $[C(\Omega)]$ is the global asymmetric matrix including an antisymmetric gyroscopic matrix (function of Ω speed of rotation) and a frequently asymmetric matrix due to the characteristics of the bearings, $[K]$ is the elastic stiffness matrix that is frequently asymmetric due to the characteristics of bearings, $\{F(t)\}$ is the generalized force vector and $\left\{\ddot{d}\right\}$, $\left\{\dot{d}\right\}$ and $\{d\}$ are respectively nodal acceleration, velocity and displacement vectors. Taking into account the material's dissipative effects gives two other matrices associated with internal damping, as shown in Sino [22]:

$$[M]\left\{\ddot{d}\right\} + [C_i + C(\Omega)]\left\{\dot{d}\right\} + [K + K_i(\Omega)]\{d\} = \{F(t)\} \tag{2}$$

where $[C_i]$ is the internal damping matrix and $[K_i(\Omega)]$ a stiffness matrix which depends on the internal damping and also on the rotational speed Ω. The anisotropic properties of composite materials and their lightness can be used to optimize composite shafts in order to improve their dynamic behavior. Compared to metals, composite materials have higher damping capacities which can induce a destabilizing effect on the rotor motion. When modeling composite rotors with the equivalent modulus beam theory, equations (1) and (2) are considered directly. However, as mentioned earlier, this approach is based on symmetric stacking laminate theory and cannot take into account the influence of layer stacking order. In the following, a more general homogenized beam model is proposed.

3 Composite rotor

The shaft studied can be obtained by winding several plies of embedded fibers on a mandrel, as shown in figure 1. Each ply has an orthotropic mechanical behavior, as shown in figure 2. The generalized Hooke's law for an orthotropic material is written as follows:

$$\{\sigma\} = [Q]\{\epsilon\} \quad or \quad \{\epsilon\} = [S]\{\sigma\} \tag{3}$$

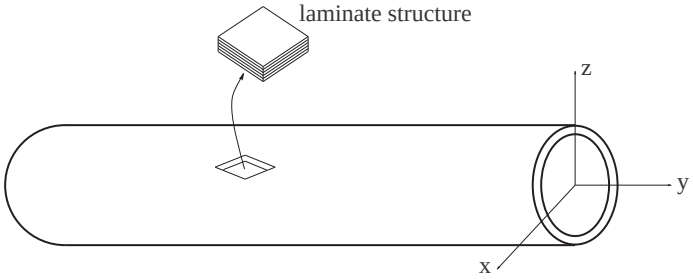

Fig. 1. Composite rotor

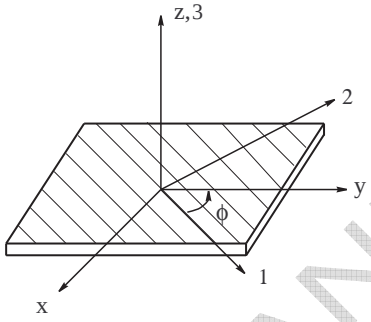

Fig. 2. Plan of ply

where $\{\sigma\}$ and $\{\varepsilon\}$ are respectively the stress and strain fields, $[Q]$ and $[S]$ are respectively the material stiffness and compliance matrices. Only the expression of the compliance matrix will be developed here. The stiffness matrix can be obtained by considering that $[Q] = [S]^{-1}$. When linked to the orthotropic axis, Hooke's law takes the following form:

$$\begin{Bmatrix} \varepsilon_1 \\ \varepsilon_2 \\ \varepsilon_3 \\ \gamma_{23} \\ \gamma_{13} \\ \gamma_{12} \end{Bmatrix} = \begin{bmatrix} 1/E_1 & -\upsilon_{21}/E_2 & -\upsilon_{31}/E_3 & 0 & 0 & 0 \\ -\upsilon_{12}/E_1 & 1/E_2 & -\upsilon_{31}/E_3 & 0 & 0 & 0 \\ -\upsilon_{13}/E_1 & -\upsilon_{31}/E_2 & 1/E_3 & 0 & 0 & 0 \\ 0 & 0 & 0 & 1/G_{23} & 0 & 0 \\ 0 & 0 & 0 & 0 & 1/G_{13} & 0 \\ 0 & 0 & 0 & 0 & 0 & 1/G_{12} \end{bmatrix} \begin{Bmatrix} \sigma_1 \\ \sigma_2 \\ \sigma_3 \\ \tau_{23} \\ \tau_{13} \\ \tau_{12} \end{Bmatrix} \quad (4)$$

where $(1, 2, 3)$ are the orthotropic axes. 1 is the fiber direction, 2 is the direction transversal to the fibers in the ply, 3 is the direction perpendicular to the ply and ϕ is the ply fiber angle. Each ply can be characterized by a plane stress state ($\sigma_{33} = 0$). Then, the above relation can be split into membrane and

transverse shear effects:

$$\begin{Bmatrix} \varepsilon_1 \\ \varepsilon_2 \\ \gamma_{12} \end{Bmatrix} = \begin{bmatrix} 1/E_1 & -\upsilon_{21}/E_2 & 0 \\ -\upsilon_{12}/E_1 & 1/E_2 & 0 \\ 0 & 0 & 1/G_{12} \end{bmatrix} \begin{Bmatrix} \sigma_1 \\ \sigma_2 \\ \tau_{12} \end{Bmatrix} \tag{5}$$

$$\begin{Bmatrix} \gamma_{23} \\ \gamma_{13} \end{Bmatrix} = \begin{bmatrix} 1/G_{23} & 0 \\ 0 & 1/G_{13} \end{bmatrix} \begin{Bmatrix} \tau_{23} \\ \tau_{13} \end{Bmatrix} \tag{6}$$

The following parameters have to be identified for each ply: E_1 and E_2 Young moduli in the orthotropic axes; G_{23}, G_{13}, G_{12}, transversal shear moduli, and ν_{12} and ν_{21} Poisson's ratios. When considering the transversal shear effects, it is often very difficult to obtain an estimation of shear moduli G_{23} and G_{13}, therefore it is often assumed that they have the same value as G_{12}. The behavior of a viscoelastic composite material in harmonic steady-state motion can be described by the complex constitutive relation. Assuming cyclic loading, the complex stress component is written as:

$$\{\sigma\} = ([Q] + j\,[Q^*])\,\{\epsilon\} \tag{7}$$

with $[Q^*] = [Q][\eta]$, $[\eta]$ is the damping matrix of the ply and j is the imaginary unit. The dissipative properties of a ply can also be expressed by using the specific damping capacities matrix $[\Psi]$. Usually energy dissipation in solids is characterized by the relative energy dissipation which is defined as the ratio of the energy losses $\triangle W$ in a unit volume of a body, to the elastic energy W under a given stress-strain state, Zinoviev [25]:

$$\psi = \frac{\Delta W}{W} = \frac{\int_0^{\pi/2\omega} \{\epsilon\}^t\ [S^*]\,\{\epsilon\}\,dt}{\int_0^{\pi/2\omega} \{\epsilon\}^t\ [S]\,\{\epsilon\}\ dt} \tag{8}$$

where $[S^*]$ is the damped compliance matrix. The composite ply has three main directions of specific damping capacity, which can be expressed by the following matrix.

$$[\Psi]_m = \begin{bmatrix} \psi_1 & 0 & 0 \\ 0 & \psi_2 & 0 \\ 0 & 0 & \psi_{12} \end{bmatrix} \ and\ [\Psi]_s = \begin{bmatrix} \psi_{23} & 0 \\ 0 & \psi_{13} \end{bmatrix} \tag{9}$$

Here ψ_1, ψ_2 and ψ_{12} are the specific damping capacities associated with the membrane effects in the orthotropic axes, and ψ_{23} and ψ_{13} are those asso-

ciated with the transversal shear effect. These coefficients can be identified experimentally. The damping matrix $[\eta]$ can be linked to the specific damping capacity as follows:

$$[\eta]_m = \frac{1}{2\pi}\begin{bmatrix} \psi_1 & 0 & 0 \\ 0 & \psi_2 & 0 \\ 0 & 0 & \psi_{12} \end{bmatrix} \; and \; [\eta]_s = \frac{1}{2\pi}\begin{bmatrix} \psi_{23} & 0 \\ 0 & \psi_{13} \end{bmatrix} \tag{10}$$

where $[\eta]_m$ and $[\eta]_s$ are membrane and shear damping matrices respectively. Consequently, the damped material stiffness matrix $[Q^*]$ is expressed as a function of the specific damping capacity as follows $[Q^*] = \frac{1}{2\pi}[Q][\psi]$. All the above equations are written in the orthotropic axes. Each ply p is positioned by the angle ϕ_p between the y and 1 axes (shaft and fiber axes). They are written in the global frame (x, y, z) by using the following transformations:

$$\{\sigma\}_{1,2} = [T]\{\sigma\}_{x,y} \quad , \{\epsilon\}_{1,2} = [T]^{-t}\{\epsilon\}_{x,y} \quad , [S]_{x,y} = [T]^t [S]_{1,2} [T]$$
$$[Q]_{x,y} = [T]^{-t}[Q]_{1,2}[T]^{-1} \; , [Q^*]_{x,y} = [T]^{-t}[Q^*]_{1,2}[T]^{-1},$$

where the transfer matrix $[T]$ is given by:

$$[T] = \begin{bmatrix} c^2 & s^2 & -2cs \\ s^2 & c^2 & 2cs \\ sc & -sc & (c^2 - s^2) \end{bmatrix} \tag{11}$$

with $c = \cos(\phi_p)$ and $s = \sin(\phi_p)$. Then, the compliance matrix takes the following form and coupling terms appear in the third column and line.

$$\begin{Bmatrix} \varepsilon_x \\ \varepsilon_y \\ \gamma_{yx} \end{Bmatrix} = \begin{bmatrix} 1/E_x & -\upsilon_{yx}/E_y & \eta_{xy}/G_{xy} \\ -\upsilon_{xy}/E_x & 1/E_y & \mu_{xy}/G_{xy} \\ \eta_x/E_x & \mu_y/E_y & 1/G_{xy} \end{bmatrix} \begin{Bmatrix} \sigma_x \\ \sigma_y \\ \tau_{xy} \end{Bmatrix} \tag{12}$$

$$\begin{Bmatrix} \gamma_{xz} \\ \gamma_{yz} \end{Bmatrix} = \begin{bmatrix} 1/G_{xz} & 0 \\ 0 & 1/G_{yz} \end{bmatrix} \begin{Bmatrix} \tau_{xz} \\ \tau_{yz} \end{Bmatrix} \tag{13}$$

Membrane strain is $\{\epsilon\}_m = [S]_m\{\sigma\}_m$ and shear strain is $\{\epsilon\}_s = [S]_s\{\sigma\}_s$, where $[S]_m$, $[S]_s$ are membrane and shear compliance matrices, and $\{\sigma\}_m$, $\{\sigma\}_s$ are membrane and shear stresses respectively.

The elastic and damping properties of the orthotropic ply are now established. The following paragraph presents the formulation used to determine the equations of motion of the composite rotor, including dissipative effects.

4 Expression of energies

Let' s consider a multilayered composite shaft made of N orthotropic layers. If the stacking sequence is symmetric the shaft has a typical beam behavior and can be modeled by using classical beam theory associated the homogenized stiffness parameters. If the stacking sequence is nonsymmetric, mechanical coupling effects such as bending-stretching, twisting-stretching and shear-stretching will be present. In this study, we assume that coupling effects are negligible.

Let's consider a beam theory to model the composite rotor illustrated in figure 1. Thus the shaft is modeled as a beam with a constant circular cross-section. The finite element used has two nodes as shown in figure 3. For each node, the element has four degrees of freedom: two displacements u and w, and two slopes about the x and z axes denoted respectively θ_x and θ_z. In this case, the beam axis is y. The continuous displacement field at material points along the

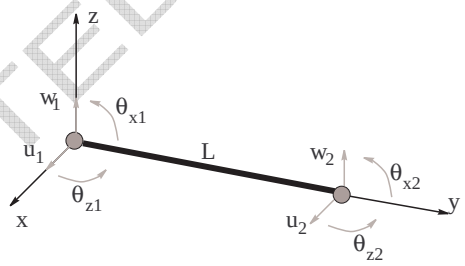

Fig. 3. Beam finite element

rotor cross-section is described as follows:

$$\{u(x,y,z)\} = \begin{cases} u_x(x,y,z) = u(y) \\ u_y(x,y,z) = -z\theta_x(y) + x\theta_z(y) \\ u_z(x,y,z) = w(y) \end{cases} \tag{14}$$

Hence, the deformation field has the following form:

$$\{\epsilon\} = \begin{cases} \varepsilon_{yy} = -z\frac{\partial\theta_x}{\partial y} + x\frac{\partial\theta_z}{\partial y} \\ \gamma_{yz} = -\theta_x + \frac{\partial w}{\partial y} \\ \gamma_{yx} = \theta_z + \frac{\partial u}{\partial y} \end{cases} \tag{15}$$

Beam theory assumes that $\sigma_{xx} = \sigma_{zz} = \sigma_{xz} = 0$. Consequently, for each ply p of the rotor cross-section, the stress-strain relation is written as:

$$\{\sigma\}^p = \begin{cases} \sigma^p_{yy} = E^p_y \varepsilon_{yy} + E^{*p}_y \dot{\varepsilon}_{yy} \\ \tau^p_{yz} = G^p_{yz}\gamma_{yz} + G^{*p}_{yz}\dot{\gamma}_{yz} \\ \tau^p_{yx} = G^p_{yx}\gamma_{yx} + E^{*p}_y \dot{\gamma}_{yx} \end{cases} \tag{16}$$

where E^p_y, G^p_{yz} and G^p_{yx} are respectively Young's modulus and transversal shear moduli. E^{*p}_y,G^{*p}_{yz} and G^{*p}_{yx} are the associated moduli linked to damping, according to the rotor axis y. with:

$$E^p_y = \frac{1}{\frac{c^4}{E^p_l} + \frac{s^4}{E^p_t} + c^2 s^2 \left(\frac{1}{G^p_{lt}} - 2\frac{\upsilon^p_{tl}}{E^p_t}\right)}, \; c = \cos(\phi_p), \; s = \sin(\phi_p) \tag{17}$$

Then the stress vector can be split into elastic stress $\{\sigma\}^p_e$ and dissipative stress $\{\sigma^*\}^p_d$:

$$\{\sigma\}^p = \{\sigma\}^p_e + \{\sigma^*\}^p_d \tag{18}$$

Using equation (16), the two parts of (18) become:

$$\{\sigma\}^p_e = \begin{cases} \sigma^p_{yy} = E^p_y \left(-z\frac{\partial\theta_x}{\partial y} + x\frac{\partial\theta_z}{\partial y}\right) \\ \tau^p_{yz} = G^p_{yz}\left(-\theta_x + \frac{\partial w}{\partial y}\right) \\ \tau^p_{yx} = G^p_{yx}\left(\theta_z + \frac{\partial u}{\partial y}\right) \end{cases} \tag{19}$$

$$\{\sigma^*\}^p_d = \begin{cases} \sigma^{*p}_{yy} = E^{*p}_y \left(-z\frac{\partial\dot{\theta}_x}{\partial y} + x\frac{\partial\dot{\theta}_z}{\partial y}\right) \\ \tau^{*p}_{yz} = G^{*p}_{yz}\left(-\dot{\theta}_x + \frac{\partial \dot{w}}{\partial y}\right) \\ \tau^{*p}_{yx} = G^{*p}_{yx}\left(\dot{\theta}_z + \frac{\partial \dot{u}}{\partial y}\right) \end{cases} \tag{20}$$

where σ^p_{yy} and σ^{*p}_{yy} are the normal cross-section stresses, τ^p_{yz}, τ^{*p}_{yz} and τ^p_{yx}, τ^{*p}_{yx}

are the transverse shear stresses. The elastic energy of the rotor can be written as:

$$U = \frac{1}{2}\int_0^L \int_S \left(\sigma_{yy}^p \varepsilon_{yy} + \tau_{yz}^p \gamma_{yz} + \tau_{yx}^p \gamma_{yx}\right) dSdy \tag{21}$$

with S being the cross section. The virtual dissipative work has the following expression:

$$\delta W = \int_0^L \int_S \left(\sigma_{yy}^{*p} \delta\varepsilon_{yy} + \tau_{yz}^{*p} \delta\gamma_{yz} + \tau_{yx}^{*p} \delta\gamma_{yx}\right) dSdy \tag{22}$$

Equation (21) can be explicitly written as a function of displacement field components (15) and (19).

$$\begin{aligned} U = &\frac{1}{2}\int_0^L \int_S E_y^p \left(z^2 (\frac{\partial \theta_x}{\partial y})^2 + x^2 (\frac{\partial \theta_z}{\partial y})^2\right) dSdy \\ &+ \frac{1}{2}\int_0^L \int_S \left[G_{yz}^p \left(-\theta_x + \frac{\partial w}{\partial y}\right)^2 + G_{yx}^p \left(\theta_z + \frac{\partial u}{\partial y}\right)^2\right] dSdy \end{aligned} \tag{23}$$

The virtual work can also be expressed as a function of the stress field components by using equation (16). Thus equation (22) becomes:

$$\delta W = \int_0^L \int_S E_y^{*p}\, \dot{\varepsilon}_{yy}\, \delta\varepsilon_{yy}\, dSdy + \int_0^L \int_S \left(G_{yz}^{*p} \dot{\gamma}_{yz} + G_{yx}^{*p} \dot{\gamma}_{yx}\right) \delta\gamma\, dSdy \tag{24}$$

By using equation (20), equation (24) is:

$$\begin{aligned} \delta W = &\int_0^L \int_S E_y^{*p} \left(-z\frac{\partial \dot{\theta}_x}{\partial y} + x\frac{\partial \dot{\theta}_z}{\partial y}\right)\left(-z\frac{\partial \delta\theta_x}{\partial y} + x\frac{\partial \delta\theta_z}{\partial y}\right) dSdy \\ &+ \int_0^L \int_S \left[G_{yz}^{*p} \left(-\dot{\theta}_x + \frac{\partial \dot{w}}{\partial y}\right)\left(-\delta\theta_x + \frac{\partial \delta w}{\partial y}\right)\right] dSdy \\ &+ \int_0^L \int_S \left[G_{yx}^{*p} \left(\dot{\theta}_z + \frac{\partial \dot{u}}{\partial y}\right)\left(\delta\theta_z + \frac{\partial \delta u}{\partial y}\right)\right] dSdy \end{aligned} \tag{25}$$

5 Homogenization and equation of motion

The rotor has constant geometric properties along its longitudinal y axis. The homogenized mechanical characteristics are extracted from equations (23) and (25) by evaluating the integrals over the cross-section. The potential energy and virtual work can be expressed as follows:

$$\begin{aligned} U = & \frac{1}{2}\int_0^L \left(EI_x(\frac{\partial\theta_x}{\partial y})^2 + EI_z(\frac{\partial\theta_z}{\partial y})^2 \right) dy \\ & + \frac{1}{2}\int_0^L \left[GS_{yz}\left(-\theta_x + \frac{\partial w}{\partial y}\right)^2 + GS_{yx}\left(\theta_z + \frac{\partial u}{\partial y}\right)^2 \right] dy \end{aligned} \tag{26}$$

$$\begin{aligned} \delta W = & \int_0^L \left(EI_x^* \frac{\partial\dot{\theta}_x}{\partial y}\frac{\partial\delta\theta_x}{\partial y} + EI_z^* \frac{\partial\dot{\theta}_z}{\partial y}\frac{\partial\delta\theta_z}{\partial y} \right) dy \\ & + \int_0^L \left[GS_{yz}^* \left(-\dot{\theta}_x + \frac{\partial\dot{w}}{\partial y}\right)\left(-\delta\theta_x + \frac{\partial\delta w}{\partial y}\right) \right] dy \\ & + \int_0^L \left[GS_{yx}^* \left(\dot{\theta}_z + \frac{\partial\dot{u}}{\partial y}\right)\left(\delta\theta_z + \frac{\partial\delta u}{\partial y}\right) \right] dy \end{aligned} \tag{27}$$

The rotor cross-section is circular thus the homogenized flexural inertias are $EI_z = EI_x = EI$. They are obtained from:

$$EI = \sum_{p=1}^{N} E_y^p I^p \quad \text{with} \quad I^p = \frac{R_p^4 - R_{p-1}^4}{4} \tag{28}$$

where I^p is the cross-section inertia and R_p, R_{p-1} are the external and internal radius of layer p. The homogenized shear rigidities are $GS_{yx} = GS_{yz} = GS$, with:

$$GS = k\sum_{p=1}^{N} G_{12}^p S^p \tag{29}$$

where k is the transverse shear correction factor and S^p is the cross-section area of the ply p. Shear correction factor k is determined as described in Nouri [11] by evaluating the warping shape of the rotor cross-section. The damped homogenized mechanical characteristics, i.e. flexural inertia $EI^* = EI_x^* = EI_z^*$ and shear stiffness GS^*, are extracted from the expression of the virtual

work. Using the relation between the effective membrane and shear loss factor equations, (10), and the specific damping capacity, they can be expressed as:

$$EI^* = \sum_{p=1}^{N} E_y^{*p} I^p \text{ and } GS^* = k \sum_{p=1}^{N} G_{12}^{*p} S^p \tag{30}$$

Applying Lagrange's equations to the energy expressions, leads to the equations of motion in the fixed frame as reported in equation (2). The advantage of the proposed approach is that it can be used within a classical finite beam element. The stiffness matrix $[K]$ depends on the homogenized characteristics GS and EI, and $[K_i(\Omega)]$, $[C_i]$ on the homogenized characteristics GS^* and EI^*.

6 Applications

6.1 Comparison of critical speed without internal damping

In this example we consider the shaft first studied by Zinberg and Symmonds [26] and recently by Gubran and Gupta in [19]. The fundamental natural frequency obtained in this work is compared to the experimental value and those obtained by using EMBT, modified EMBT and LBT methods. The geometric and material properties of the rotor are:

- L=2.47 m, mean radius=0.0635 m, Wall thickness=1.321 $\times 10^{-3}$ m;
- 10 layers of equal thickness from the innermost layer $[90°, 45°, -45°, [0°]_6, 90°]$;
- $\rho = 1967s\, kg/m^3$;
- $E_{11} = 210\, GPa$, $E_{22} = 24.1\, GPa$, $G_{12} = 6.9\, GPa$, $\nu_{12} = 0.36$.

Critical speed obtained by different investigators using different methods are presented in the table 1. They are compared to the experimental critical speed obtained by Zinberg and Symmonds in [26]. It appears that the greatest error is that obtained by the EMBT method. The best results are those obtained by the present work and the modified EMBT and LBT methods presented by Gubran and Gupta in [19].

Critical speed obtained by the SHBT method (including shear effect with corrector factor obtained by evaluating cross-sectional warping as shown in Nouri and Gay [11]) agrees with those of the literature: numerical and experimental. In spite of its simplicity, this method can also take into account the effect of internal material damping.

Investigator	Critical speed (rev/min)	Method
Zinberg and Symmonds [26]	5500	Experimental
	5780 (5.09 %)	Equivalent Modulus Beam Theory
Singh and Gupta [15]	5620 (2.18 %)	Layerwise Beam Theory including shear effect
Chen and Peng [3]	5714 (3.89 %)	
Gubran and Gupta [19]	5555 (1.00 %)	Layerwise Beam Theory without including Poisson effect
	5552 (0.94 %)	Modified Equivalent Modulus Beam Theory without including Poisson's effect
Present work	5767 (4.85 %)	Simplified Homogenized Beam Theory without including shear effect
	5435 (1.18 %)	Simplified Homogenized Beam Theory including shear effect (shear corrector factor $k = 0.4983$)

Table 1
Comparison of critical speed obtained by different investigators using different formulations with that obtained in this work. The error indicated in the table relates to the experimental critical speed.

6.2 Comparison of natural frequency and instability thresholds including internal damping

In this section, we study the influence of internal material damping on critical speed and instability threshold. We consider the structure, proposed by Pereira [6] which is a composite shaft with two rigid steel disks supported by two bearings at the ends, as shown in figure 4. This structure present the following geometric and material properties:

- Rotor : $L = 1.2m$, $R_o = 0.048m$, $e = 0.008m$
- Disk : $R_{dinner} = 0.048m$, $R_{douter} = 0.15m$, $h = 0.05m$
- Composite : carbon/epoxy 8 layers

The material properties of each ply (carbon/epoxy) are summarized in table 2 and the anisotropic bearing stiffness characteristics are described in table 3. The system is considered without external damping.

In order to emphasize the influence of internal damping in rotordynamic analysis, the Campbell diagram and instability threshold are determined. We analyse the sensitivity of critical speed and instability threshold with the stacking

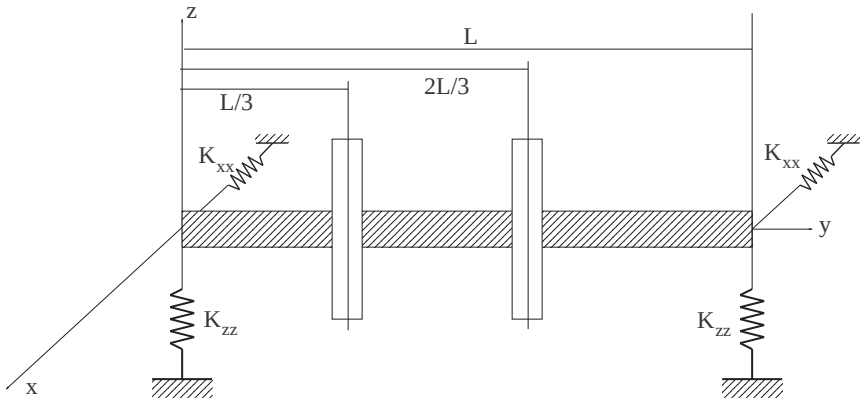

Fig. 4. Winding rotor shaft with two disks.

Material	E_1 (GPa)	E_2 (GPa)	G_{12} (GPa)	υ_{21}	ρ (kg/m^3)	ψ_1 %	ψ_2 %	ψ_{12}%
Carbon/ epoxy	172.7	7.20	3.76	0.3	1446.2	0.45	4.22	7.05

Table 2
Shaft material data

	K$_{xx}$(N/m)	K$_{zz}$(N/m)	K$_{xz}$(N/m)	K$_{zx}$ (N/m)
Anisotropic bearings	1.10^7	1.10^8	0	0

Table 3
Bearings Stiffness data

sequences and the transversal shear effect. Then, they are compared to those obtained by using the classical EMBT method.

6.2.1 Effects of stacking sequences on frequencies and instabilities

Table 4 gives the frequencies and corresponding system instability thresholds obtained from the proposed model (SHBT) with different lamination schemes in both symmetrical and asymmetrical configurations. By contrast to the EBMT method used by Pereira, the SHBT method allows considering any stacking sequence configuration. Sequences 1 and 2 have four plies at 90 $^\circ$, two plies at 45 $^\circ$ and two at 0 $^\circ$, while sequences 3 to 6 consist of four plies at 0 $^\circ$, two plies at 45 $^\circ$ and two at 90 $^\circ$. Variations of 22% for the first frequency and 48% for the associated instability threshold are obtained when comparing sequences 1 to 6. The contribution of each layer depends on its orientation with respect to the rotor axis and its distance from the longitudinal tube axis. The transversal specific damping capacity reported in table 2 shows that the

closer the fiber is oriented to 90, the greater the internal damping and the sooner instability may appear.

The Campbell diagrams shown in figures 5, 6 and 7, representing the evolution of natural frequency with respect to the speed of rotation, illustrate the significant influence of stacking sequences on frequencies and instability thresholds.

In figure 5 the composite rotor is in a balanced and symmetrical configuration: $[\pm 75^\circ]_{8S}$. In this case, instabilities (symbolized by a dashed line) occur just after the second critical speed. Such results are in perfect agreement with those obtained by Pereira [6] using the EMBT formulation. The Campbell diagrams associated with the second and the fifth sequences (table 4) are presented respectively in figures 6 and 7 and illustrate the advantage of using stacking sequences as an optimization parameter for both frequencies and instability thresholds. The differences between the two configurations is up to 21% for frequencies at rest for the first forward whirl (FW1) and about 47% for instability thresholds (5913 and 11111 rpm). For the fifth sequence, rotor speed can exceed the third critical speed without generating instability, whereas instability occurs at speeds higher than the second critical speed for the second sequence. Such behavior is explained by the fact that the greater the number of fibers oriented close to the longitudinal direction of the tube, the more they contribute to shaft rigidity and, consequently, the higher frequencies are. In parallel, the lower the orientation angle, the lower the internal damping due to the composite materials is and, consequently, the later instability occurs.

Mechanical characteristics of composite	Stacking sequence	F_1(Hz)	Instability threshold (rpm)
1	$[90_2,45,0]_S$	39.87	5864
2	[90,0,90,45,90,45,0,90]	40.08	5913
3	$[90,45,0_2]_S$	50.71	10981
4	$[0_2,45_2,90_2,0_2]$	50.91	11106
5	$[0_2,90,45]_S$	50.92	11111
6	[45,0,45,0,90,0,90,0]	51.36	11395

Table 4
Mechanical characteristics of the shaft and Results

6.2.2 Effects of transversal shear on frequencies and instability

The natural frequencies calculated by using SHBT are plotted in figure 8 with respect to rotor parameter L/R_o (ratio of length over outer radius) for the same test case made of 8 plies of 0.001 m thick in a balanced and symmetric

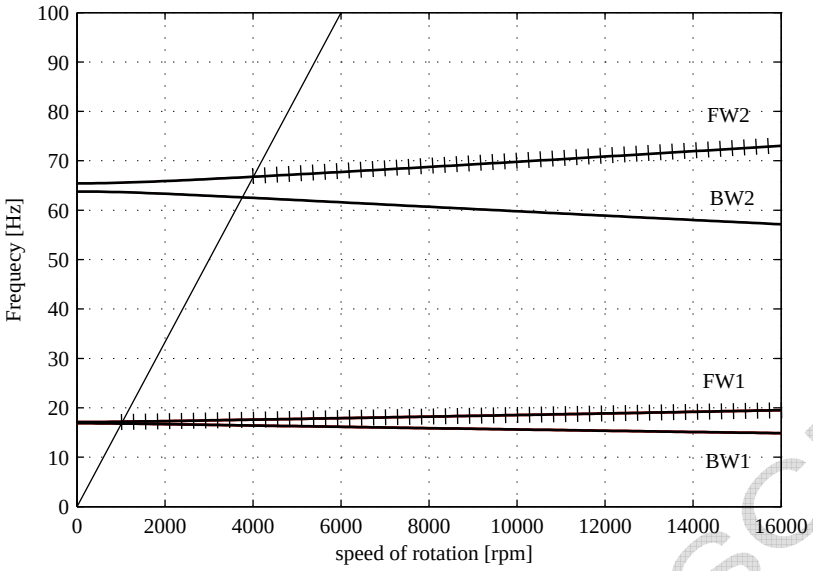

Fig. 5. Campbell diagram and instability regions for a laminate $[\pm 75^\circ]$ with anisotropic bearings

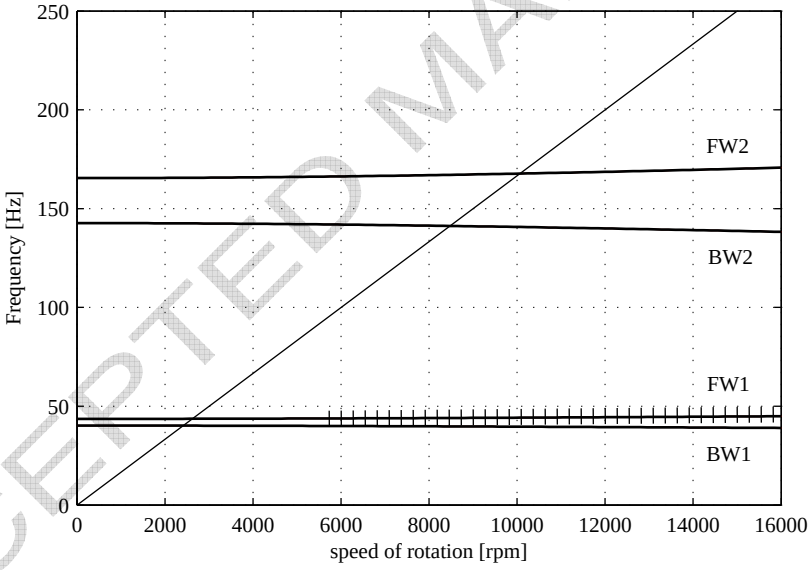

Fig. 6. Campbell diagram and instability regions with anisotropic bearings: second case $[90, 0, 90, 45, 90, 45, 0, 90]$

configuration. Results both with and without transversal shear effects are represented ('S' symbolizes transversal shear). Classically, shear deformation has an influence at low L/R_o and is significant here above the first frequency. The variation of instability thresholds with respect to ratio L/R_o is shown for a configuration $[\pm 75^\circ]_{8S}$ in figure 9 and leads to the conclusion that frequencies

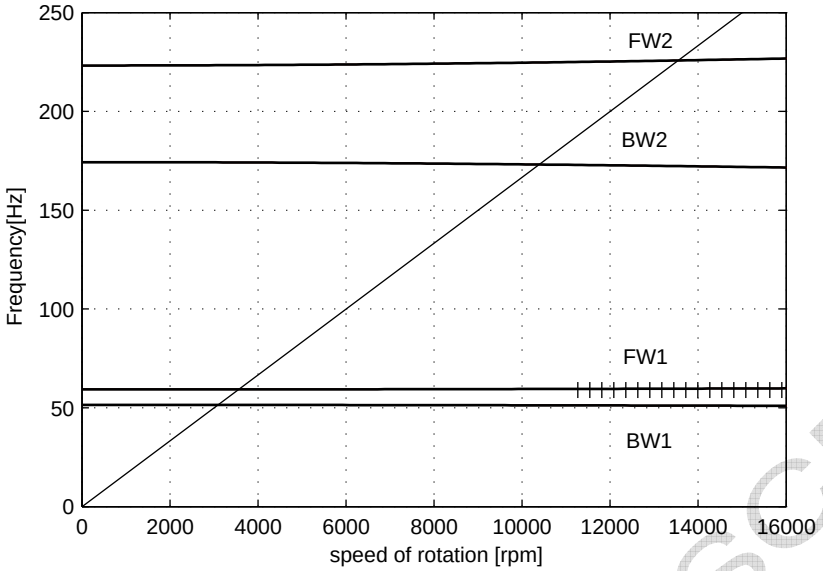

Fig. 7. Campbell diagram and instability regions with anisotropic bearings: fifth case $[0_2, 90, 45]_s$

and shear deformation decrease with L/R_o.

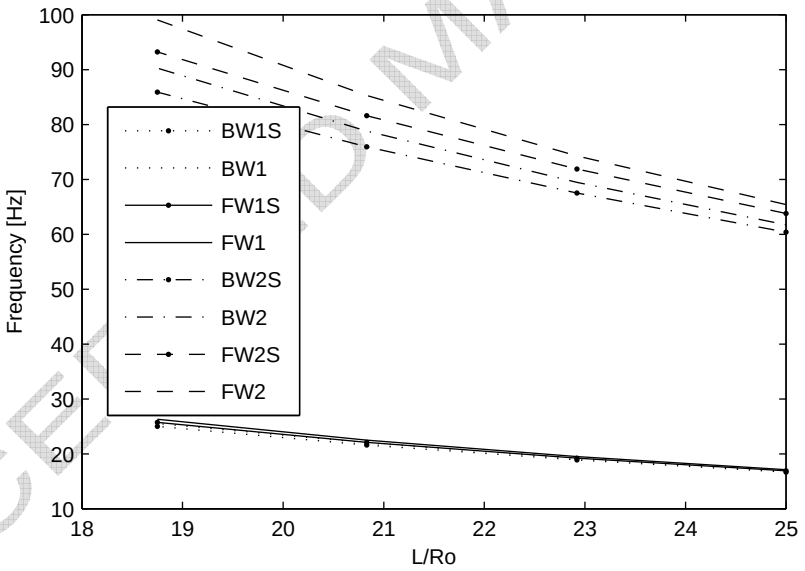

Fig. 8. Natural frequencies of a symmetrical laminate for different L/Ro ratios for $[\pm 75]$ angle orientation with and without shear effects

Tables 5 and 6 give the frequencies and the instability thresholds with respect to the ply angle for a specific value of L/R_o=20.83, in order to demonstrate the influence of angle orientation. Table 5 shows that frequencies increase as the fiber angle decreases. The system is stiffer when fibers are directed

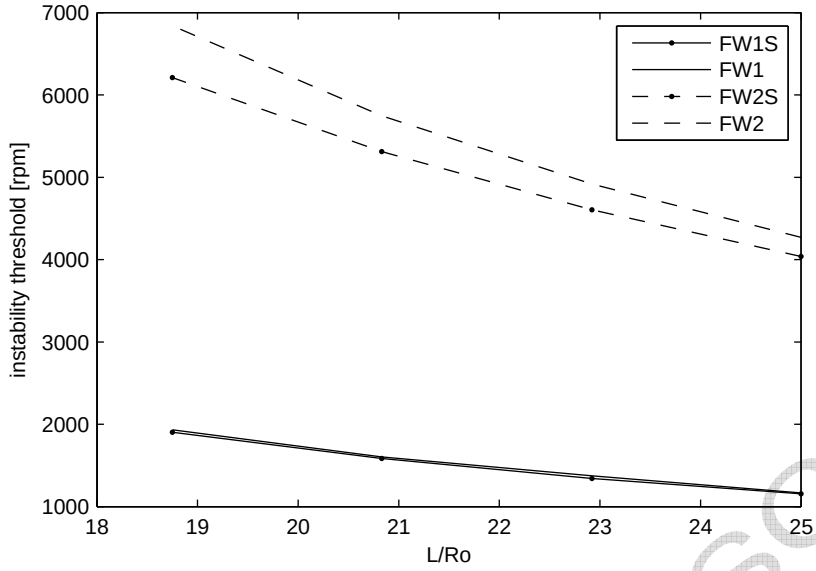

Fig. 9. Instability threshold for different L/Ro ratios for [±75] angle orientation with and without shear effects

mostly along the shaft axis. Thus internal damping decreases as the frequencies increase (longitudinal specific damping capacity is lower than the transversal specific damping capacity), leading to an increase in the instability threshold. Table 6 confirms this conclusion, highlighting that equivalent rigidity decreases as a function of ply angle whereas the damped equivalent rigidity increases.

Considering the first two forward precessions, the error made when neglecting shear effects is 2% for the first flexural frequency and 7.5% for the second flexural frequency for orientation $[\pm 75^\circ]_s$. This error increases by up to 11% and 33.5% for the first and the second frequencies respectively with orientation $[\pm 15^\circ]_s$.

θ (Degrees)	$FW1\ (Hz)$	$FW2\ (Hz)$	$FW1s\ (Hz)$	$FW2s\ (Hz)$
[±15]	61.55	229.57	54.37	152.49
[±45]	28.55	108.09	27.73	95.72
[±75]	22.49	85.27	22.08	78.81

Table 5
Natural frequencies of a symmetrical laminate for different ply angles with and without shear effects with L/Ro=20.83

6.2.3 Comparative study of the two homogenization methods

A comparative study between the proposed SHBT and EMBT methods is carried out. When considering a composite rotor in a balanced and symmetric

ϕ (Degrees)	EI ($N\,m^2$)	$EI\eta$	Instability threshold with shear (rmp)	Instability threshold without shear(rpm)
[±15]	97811	136	10404	9937
[±45]	21206	277	2309	2255
[±75]	15717	338	1604	1585

Table 6
Mechanical characteristics of the shaft and instability thresholds

configuration $[\pm 75^\circ]_{8S}$ (figure 5), the frequencies and instability thresholds obtained with both methods are in very good agreement. On the other hand, the results associated with the different stacking configurations listed in table 7 demonstrate that the distance to the neutral axis contributes to the calculation of the mechanical characteristics of the rotor with SHBT, but not accurately with EMBT as mentioned by Singh and Gupta in [14,15]. When using EMBT, a difference of 15.7% and 15.1% in the instability threshold and 6.7% and 6.3% in the first frequencies is observed for sequences 2 and 3. This difference is more important than that obtained for critical speed. Obviously, the modified EMBT and LBT methods developed by Gubran and Gupta could give better results than classical EMBT, if internal damping is taken into account.

Stacking sequence	Instability threshold (rpm)		Error (%)	F1(Hz)		Error (%)
	SHBT	EMBT		SHBT	EMBT	
$[\pm 75^\circ]_{8S}$	1167	1167	0	16.88	16.88	0
$[90_2,45,0]_S$	5864	6956	15.7	39.87	42.76	6.7
[90,0,90,45,90,45,0,90]	5913	6965	15.1	40.08	42.76	6.3
$[90,45,0_2]_S$	10981	12064	9	50.71	52.37	3.2
$[0_2,45_2,90_2,0_2]$	11106	12064	8	50.91	53.37	3
$[0_2,90,45]_S$	11111	12064	8	50.92	52.37	3
[45,0,45,0,90,0,90,0]	11395	12064	5.5	51.36	52.37	2

Table 7
Comparison between SHBT and EMBT

For sequences 4 to 7, this error is 9% for the instability threshold and 3.2% for the frequencies. Consequently, the classical EMBT over-estimates the instability of the rotor.

7 CONCLUSION AND PERSPECTIVES

This work deals with the stability analysis of an internally damped rotating composite shaft. A Simplified Homogenized Beam Theory (SHBT) is developed and compared to the classical Equivalent Beam Modulus Theory (EMBT), the Modified Equivalent Beam Modulus Theory (modified EMBT) and the Layerwise Beam Theory (LBT). The method developed avoids the main drawbacks associated with EMBT formulation, that considers only symmetrical and balanced stacking sequences and does not take into account the distance of composite layers from the neutral axis. It also takes into account internal damping by using the specific damping capacity of each ply of the composite assembly, and also considers transversal flexural shear. It allows the use of existing beam finite element.

The critical speeds obtained by the method developed are in good agreement with those obtained by LBT and modified EMBT as well as the experimental one. The study highlights that EMBT simplifications may lead to significant discrepancies in terms of frequencies. These discrepancies appear to be greater for instability thresholds. A qualitative study of the effects of various parameters on frequencies and instability thresholds was carried out. The analysis shows that although transversal shear has a minor influence on the first frequencies, its effect is much more significant for the following ones, thereby directly influencing instability thresholds.

However, this method requires some improvements to take account of the coupling effects induced by nonsymmetrical stacking. These improvements will be the subject of a forthcoming paper.

References

[1] Bauchau O., 1983, Optimal Design of High Speed Rotating Graphite/Epoxy Shafts, Journal of Composite Materials, vol. 17(3), pp. 170-181.

[2] Chatelet E., Lornage D. and Jacquet-Richardet G., 2000, Dynamic behavior of thin-walled composite shafts: A three dimensional approach, 5th annual Engineering System Design and Analysis Conference, ASME, Montreux Switzerland, pp. 1-5.

[3] Chen L. W. and Peng W. K., 1998, Dynamicstability of rotating composite shafts under periodic axial compressive loads, Journal of Sound and Vibration, 212(2),215-230.

[4] Darlow M.S. and Creonte J., 1995, Optimal design of composite helicopter power transmission shafts with axially varying fiber lay-up, Journal of the American Helicopters society, vol. 40(2), pp. 50-56.

[5] Gay D., 1991, matériaux composites, Hermès.

[6] Pereira J. C. and M. E. Silveira, 2002, Evaluation and Optimization of the instability regions on rotors in wounding shaft, II Congresso Nacional de Engenharia Mecânica, João Pessoa.

[7] Kimball A.L., 1925, Internal friction as a cause of shaft whirling, Philosophical Magazine, Series 6, vol. 49(1), pp. 724.

[8] Lalanne M. and Ferraris G., 1998, Rotordynamics Prediction in Engineering, 2nd edition, J. Wiley and Sons.

[9] Bucciarelli L.L., 1982, On the Instability of Rotating Shafts due to Internal Damping, Journal of Applied Mechanics, Vol. 49, pp. 425.

[10] Newkirk B.L., 1924, Shaft Whipping, General Electric Review, vol. 27(3), pp. 169-178.

[11] Nouri T. and Gay D., 1994, Shear Stresses in Orthotropic Composite Beams, International Journal of Engineering Science, Vol. 32(10), pp. 1647-1667.

[12] Singh S.P. and Gupta, K., 1994, Free damped flexural vibration analysis of composite cylindrical tubes using beam and shell theories, Journal of Sound and Vibration, Vol. 172(2), pp. 171-190.

[13] Singh S.P. and Gupta, K., 1994, Damped free vibration of layered composite cylindrical shell, Journal of Sound and Vibration, Vol. 172(2), pp. 191-209.

[14] Singh S.P. and Gupta K., 1996, Dynamic Analysis of Composite rotors, International Journal of Rotating Machinery, vol. 2(3), pp. 179-186.

[15] Singh S.P. and Gupta K., 1996, Composite shaft rotordynamic analysis using a layerwise theory, Journal of Sound and Vibration, vol. 191(5), pp. 739-756.

[16] Singh S.P. and Gupta K., 1998, Damping measurements in fiber reinforced composite rotors, Journal of Sound and Vibration, vol. 211(3), pp. 513-520.

[17] Chandra R., Singh S.P. and Gupta, K., 1999, Damping stuies in fiber-reinforced composites- a review, Composites Structures, Vol. 46, pp. 41-51.

[18] Chandra R., Singh S.P. and Gupta, K., 2003, A study of damping in fiber-reinforced composites, Journal of Sound and Vibration, Vol. 262, pp. 475-496.

[19] Gubran H.B.H and Gupta, K., 2005, The effect of stacking sequence and coupling mechanisms on the natural frequencies of composite shafts, Journal of Sound and Vibration, Vol. 282, pp. 231-248.

[20] Plagianakos, T. S. and Saravanos, D. A., 2003, Mechanics and finite elements for the damped dynamic characteristics of curvilinear laminates and composite shell structures, Journal of Sound and Vibration, Vol. 263, pp. 399-414.

[21] Plagianakos, T. S. and Saravanos, D. A., 2004, High-order layerwise mechanics and finite elements for the damped dynamic characteristics of sandwich composite beams, International Journal of Solids and Structures, Vol. 41, pp. 6853-6871.

[22] Sino R., Chatelet E., T.N. Baranger and G. Jaquet-Richardet, 2006, Stability analysis of internally damped rotating composite shafts considering transversal shear" Proceedings of ISROMAC - 11, Honolulu, Hawaii USA.

[23] Tsaï, S.W., 1988, Composites Design, 4th edition, Dayton, Ohio, USA.

[24] Wettergren H.L. and Olsson K.O., 1996, Dynamic Instability of A Rotating Asymmetric Shaft with Internal Viscous Damping Supported in anisotropic bearings, Journal of Sound and Vibration, Academic Press Limited, Vol. N° 195, pp. 75-84.

[25] Zinoviev A. and Ermakov N., 1994, Energy Dissipation in Composite Materials, Technic publishing company, Inc., Pennsylvania U.S.A.

[26] Zinberg H. and Symmonds M.F., 1970, The development of advanced composite tail rotor driveshaft, 26th Annual National Forum of American Helicopter Society, Washington, DC, pp. 1-14.

[27] Zorzi, E.S. and Giordano, J.C., 1985, Composite Shaft Rotordynamic Evaluation, *The American Society of Mechanical Engineers*, Vol. 85-det-114.